Thin Solid Films 519 (2010) 1213–1218

Contents lists available at ScienceDirect

Thin Solid Films

journal homepage: www.elsevier.com/locate/tsf

Antibody immobilized cysteamine functionalized-gold nanoparticles for aflatoxin detection

Aditya Sharma [a], Zimple Matharu [a], G. Sumana [a], Pratima R. Solanki [a], C.G. Kim [b], B.D. Malhotra [a,b,*]

[a] Department of Science and Technology Centre on Biomolecular Electronics, Biomedical Instrumentation Section, Materials Physics and Engineering Division, National Physical Laboratory (Council of Scientific and Industrial Research), Dr. K. S. Krishnan Marg, New Delhi-110012, India
[b] Centre for NanoBioEngineering and Spintronics, Chungnam National University, Daejeon, 305-764, Republic of Korea

ARTICLE INFO

Available online 25 August 2010

Keywords:
Aflatoxin
Cysteamine
Gold nanoparticles
Immunosensor
Self assembled monolayer

ABSTRACT

Aflatoxin B_1 antibody ($aAFB_1$) covalently attached to cysteamine functionalized-gold nanoparticles (C-AuNP) has been immobilized onto 4-mercaptobenzoic acid (MBA) based self assembled monolayer (SAM) on gold electrode (MBA/Au), for the fabrication of BSA/$aAFB_1$-C-AuNP/MBA/Au immunoelectrode. This immunoelectrode has been characterized by Fourier Transform Infrared Spectroscopy (FT-IR), Scanning Electron Microscopy (SEM) and electrochemical characterization techniques. The electrochemical response studies reveal that the BSA/$aAFB_1$-C-AuNP/MBA/Au immunoelectrode can be used to detect AFB_1 in the range of 10–100 ng dL^{-1} and has sensitivity as 0.45 μA ng^{-1} dL, limit of detection as 17.90 ng dL^{-1} and a response time of 60 s.

1. Introduction

Aflatoxin B_1 (AFB_1) is the most common mycotoxin produced by strains of *Aspergillus flavus* and *Aspergillus parasiticus* that grow on food crops during their production and storage. It exhibits carcinogenic, teratogenic, mutagenic and immunosuppressive properties and has been regarded as a human carcinogen by the International Agency for Research on Cancer [1]. European Community legislation has established 2 μg of AFB_1 as the maximum amount permitted per kg (2 ppb) [2], above which it results in toxic manifestations leading to liver cancer (hepatocellular carcinoma), which is the fifth most commonly occurring cancer in the world and the third greatest cause of cancer mortality [3]. AFB_1 cannot be entirely avoided or eliminated from foods and feeds even by the current agronomic and manufacturing processes [4]. The monitoring of its concentration prior to intake is of paramount importance. Though, current analytical techniques used for the detection of AFB_1 such as thin-layer chromatography (TLC) [5] and high-performance liquid chromatography (HPLC) [6] are sensitive, but they typically require skilled operators, extensive sample pre-treatment, expensive equipment and are time-consuming [7]. The measurement of antibody or antigen concentrations based on biospecific recognition interactions such as immunoassay and biosensors, has been considered a major analytical method used in clinical diagnosis, environment, and biochemical studies and has generated much interest due to its cost-effectiveness, sensitivity and specificity [8].

Gold nanoparticles (AuNPs) due to their non-toxic nature and excellent biological compatibility have recently attracted significant attention for a variety of biomedical applications, including biosensors [9,10]. Colloidal gold layer not only increases the amount of biomolecules immobilized on the surface [11] but is also a useful interface for the electrocatalysis of redox processes of molecules by facilitating electron transfer between redox proteins and bulk electrode material. Nano-scale surfaces of AuNPs have recently been used for obtaining enhanced sensitivity of immunosensors [12] and thus are frequently used for the fabrication of desired immunosensors.

Liu et al. have fabricated microcomb electrode using self-assembly of horseradish peroxidase (HRP) and anti-AFB_1 onto AuNPs functionalized biorecognition surfaces [13]. Liao has demonstrated that nanogold hollow ball can potentially be used as matrix for the fabrication of a high affinity immunoassay by immobilizing anti-aflatoxin B_1 as a model protein [14]. In a recent communication, Jin et al. have used indirect competitive immunoassay technique for AFB_1 detection and have employed gold nanoparticles (GNP) as a 'weight label' to the secondary antibody for amplifying the response [15]. In the present manuscript we report results of the studies relating to the fabrication of gold nanoparticles based immunoelectrode by utilizing amino terminal of cysteamine functionalized AuNPs (C-AuNP) for immobilization of $aAFB_1$ in the solution phase ($aAFB_1$-C-AuNP) in order to enhance the antibodies loading onto AuNP surface. The $aAFB_1$-C-AuNP modified MBA/Au electrode has further been explored for aflatoxin B_1 (AFB_1) detection using specific anti-aflatoxin ($aAFB_1$)–aflatoxin (AFB_1) interactions.

* Corresponding author. Department of Science and Technology Centre on Biomolecular Electronics, National Physical Laboratory, Dr. K. S. Krishnan Marg, New Delhi-110012, India. Tel.: +91 11 45609152.
E-mail address: bansi.malhotra@gmail.com (B.D. Malhotra).

0040-6090/$ – see front matter © 2010 Elsevier B.V. All rights reserved.
doi:10.1016/j.tsf.2010.08.071

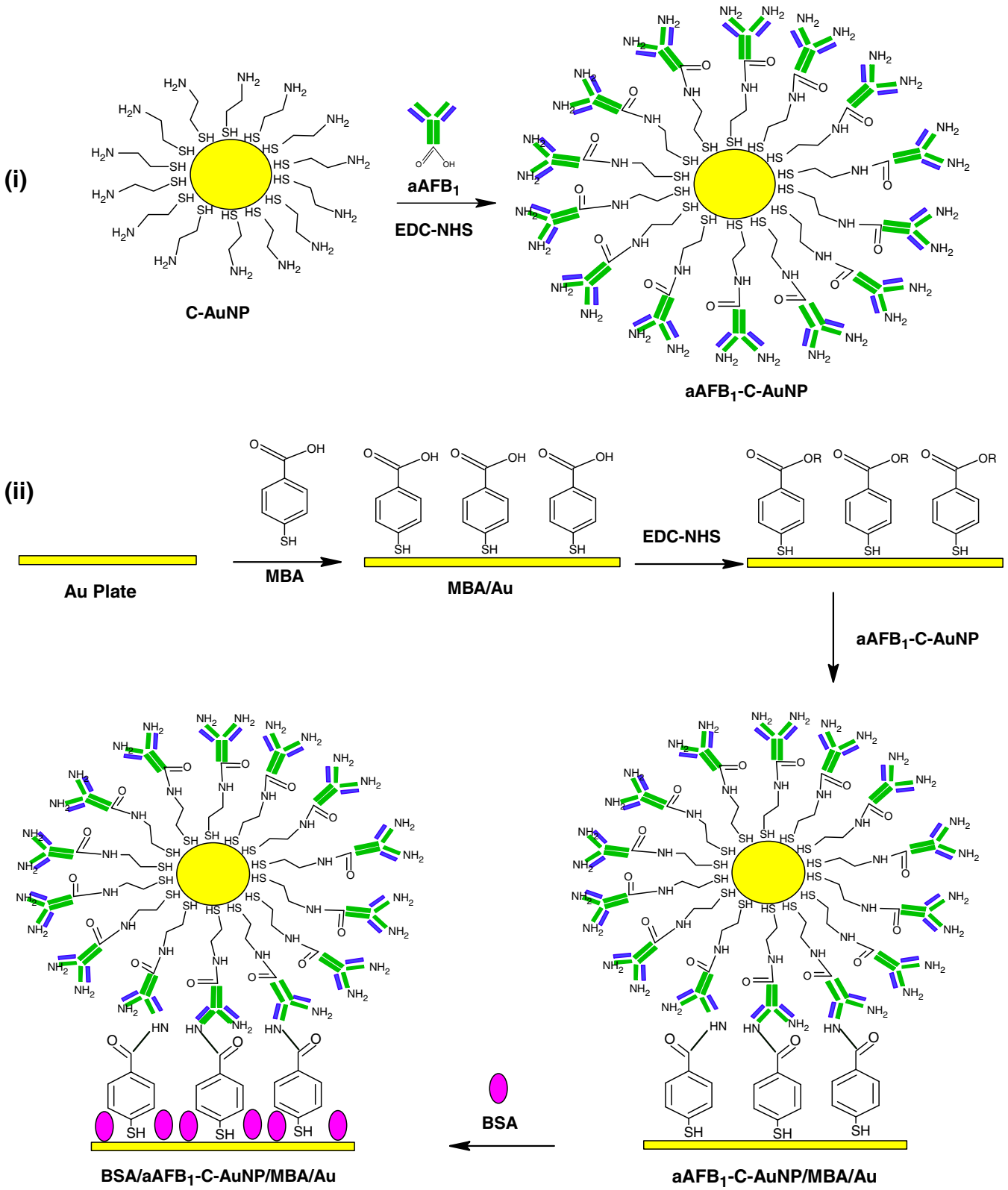

Scheme 1. Fabrication of BSA/aAFB$_1$-C-AuNP/MBA/Au immunoelectrode.

2. Experimental section

2.1. Chemicals and reagents

Hydrogen tetrachloroaurate (III) ($HAuCl_4.3H_2O$), aflatoxin B_1 (AFB_1), anti-aflatoxin B_1 mouse monoclonal antibody ($aAFB_1$), mercaptobenzoic acid (MBA) cysteamine hydrochloride, bovine serum albumin (BSA), N-hydroxysuccinimide (NHS) and N-ethyl-N′-(3-dimethylaminopropyl) carbodiimide (EDC) were purchased from Sigma-Aldrich (USA). All other chemicals were of analytical grade and were used without further purification. De-ionized water (18 MΩ cm) was used for the preparation of buffer solutions.

2.2. Preparation of solutions

The AFB_1 solution was prepared in phosphate buffer (50 mM, pH 7.0) with 10% methanol and $aAFB_1$ was prepared in phosphate buffer (50 mM, pH 7.0). Both the solutions containing 0.15 M NaN_3 as a preservative were aliquoted and stored at −20 °C. Bovine serum albumin (BSA, 98%) dissolved in phosphate buffer (2 mg/mL, pH 7.4) was used for the blocking of non-specific binding sites.

2.3. Synthesis of cysteamine functionalized-gold nanoparticles (C-AuNP)

AuNPs were prepared by adding 2 mL 1% (w/w) of sodium citrate to a boiling solution of 50 mL (0.01% w/w) $HAuCl_4$ [16]. AuNPs thus obtained were functionalized with cysteamine by treating it with 10^{-3} M aqueous solution of cysteamine hydrochloride. Aging of cysteamine and gold hydrosol in 1:9 volume ratios for 12 h at room temperature yielded C-AuNP, which were separated and purified by repeated centrifugation at 10,000 rpm for 10 min followed by washing with milliQ water.

2.4. Covalent immobilization of $aAFB_1$ onto cysteamine functionalized-gold nanoparticles ($aAFB_1$-C-AuNP)

Cysteamine functionalized-gold nanoparticles were dispersed in phosphate buffer solution of pH 7.4. $aAFB_1$ (1 mg/mL) and C-AuNP solutions were then mixed in 1:3 (v/v) ratio followed by addition of 0.2 M EDC and 0.05 M NHS for the activation of –COOH group present in $aAFB_1$. The activated carboxyl group then binds with the $–NH_2$ group of C-AuNP leading to formation of amide bond (Scheme 1(i)). The $aAFB_1$-bound gold nanoparticles were collected by centrifugation followed by washing with phosphate buffer (pH 7.4) several times. The $aAFB_1$-C-AuNP assembly was redispersed in phosphate buffer solution of pH 7.4.

2.5. Preparation of BSA/$aAFB_1$-C-AuNP/MBA/Au immunoelectrode

Gold coated glass plates (0.5×1 cm^2) were cleaned with piranha solution (H_2SO_4:H_2O_2; 7:3) prior to use. These plates were incubated overnight at room temperature into 2 mM ethanolic solution of 4-mercaptobenzoic acid (MBA) for SAM formation. The electrodes were subsequently washed with ethanol followed by rinsing with water to remove any unbound MBA molecules. The SAM was activated for about 2 h using EDC-NHS chemistry. 20 μL of $aAFB_1$-C-AuNP solution was then spread over each electrode and incubated overnight at 4 °C for the amide bond formation between amino terminal of antibodies and carboxyl terminal of MBA (Scheme 1(ii)). The non-specific sites of fabricated immunoelectrode were blocked with BSA (2 mg/mL). These fabricated BSA/$aAFB_1$-C-AuNP/MBA/Au electrodes were further utilized for AFB_1 detection using electrochemical techniques.

2.6. Characterization

The prepared AuNPs and C-AuNP were characterized using UV–Vis spectrophotometer (Phoenix-2200DPCV). Fourier Transform Infrared Spectroscopy (FT-IR, Perkin-Elmer, Model 2000) and Scanning Electron Microscopy (SEM, LEO-440) were used to characterize the electrodes. Electrochemical analysis was conducted on an Autolab Potentiostat/Galvanostat (Eco Chemie, Netherlands) with BSA/$aAFB_1$-C-AuNP/MBA/Au as the working electrode, platinum foil (Pt) as the auxiliary electrode, and saturated Ag/AgCl as the reference electrode in phosphate buffer saline (PBS, 50 mM, pH 7.4, 0.9% NaCl) containing 5 mM $[Fe(CN)_6]^{3-/4-}$ mediator.

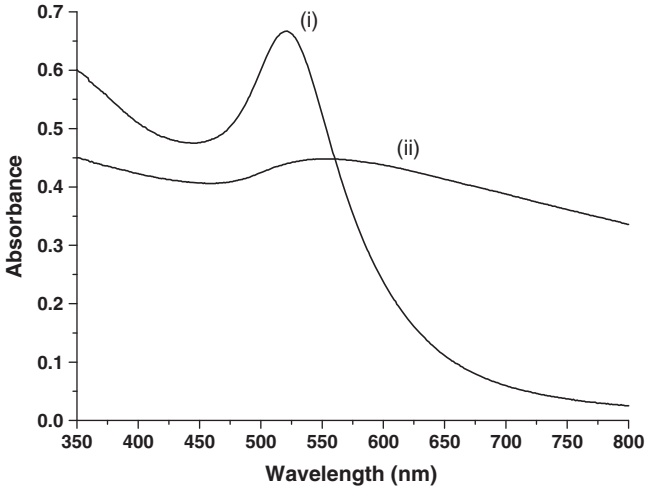

Fig. 1. UV–Visible spectra of (i) AuNPs and (ii) C-AuNP.

3. Results and discussion

3.1. UV–Visible studies

Fig. 1 shows the UV–Vis spectra of AuNPs and C-AuNP. The characteristic peak observed at 520 nm indicates the formation of

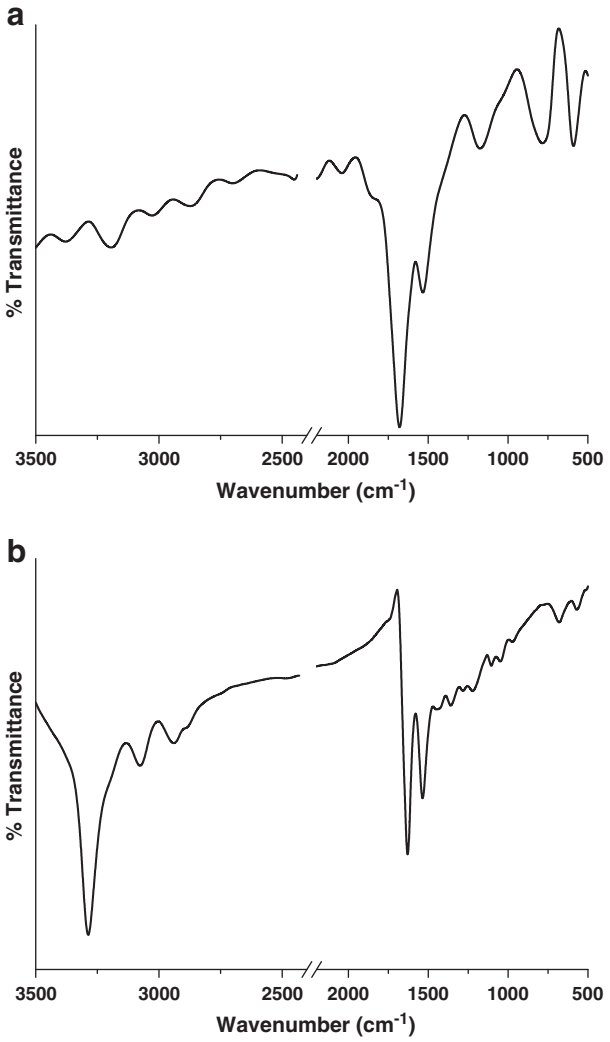

Fig. 2. FT-IR spectra of (a) MBA/Au and (b) $aAFB_1$-C-AuNP/MBA/Au electrodes.

stable gold nanoparticles (curve i) [17]. However, broadening of the peak, due to coupled plasmon resonance, along with slight shift towards higher wavelength (curve ii) indicates attachment of the cysteamine onto AuNP surface [17].

3.2. FT-IR studies

The FT-IR spectra of MBA/Au electrode show an intense peak at 1680 cm^{-1} (Fig. 2(a)), that is assigned to the carbonyl stretching of carboxylic group present in the MBA. However, after immobilization of $aAFB_1$-C-AuNP, the appearance of characteristic peaks of carbonyl stretching of amide I band at 1625 cm^{-1} and NH bending of amide II band at 1530 cm^{-1} indicates successful immobilization of the antibodies onto SAM (Fig. 2(b)). Also, a broad band seen between 3350 and 3150 cm^{-1} (curve ii) due to amide A and amide B of the protein ($aAFB_1$) further confirms the immobilization of antibodies (Fig. 2(b)).

3.3. Scanning electron microscopic studies

The results of morphological studies carried out on (a) MBA/Au and (b) $aAFB_1$-C-AuNP/MBA/Au surface are shown in Fig. 3. Plain and uniform morphology can be seen in the SEM image of MBA/Au surface (Fig 3a). However, transformation to highly dense globular morphology with bright streaks is observed after immobilization of $aAFB_1$-C-AuNP onto MBA/Au surface (Fig. 3(b)), indicating high loading of the $aAFB_1$-C-AuNP onto MBA/Au electrode.

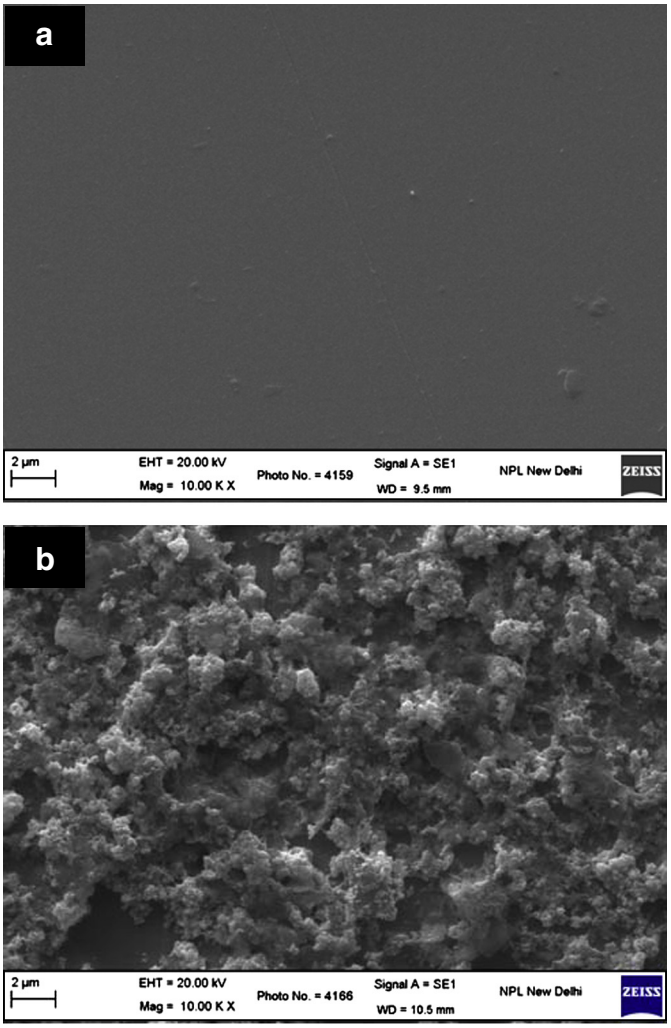

Fig. 3. Scanning electron micrograph of (a) MBA/Au SAM and (b) $aAFB_1$-C-AuNP/MBA/Au electrodes.

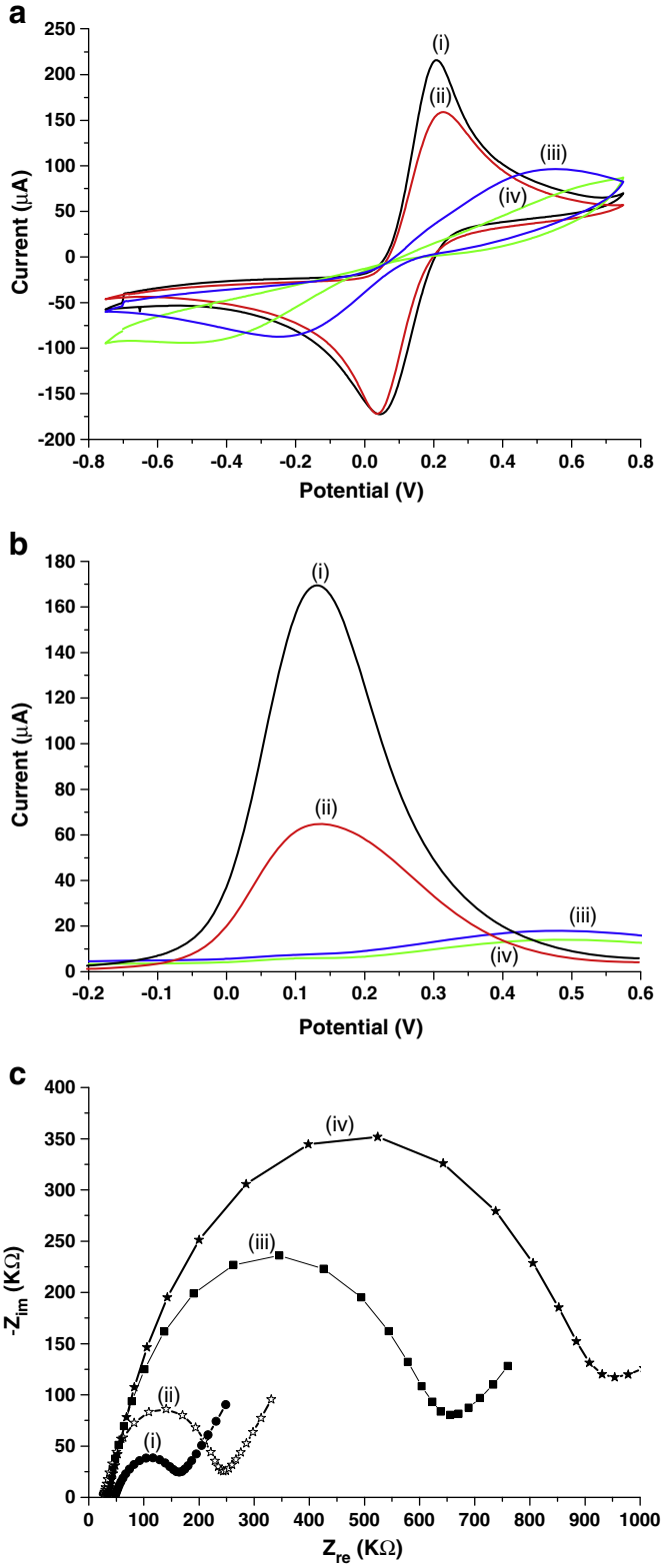

Fig. 4. (a) CV, (b) DPV and (c) EIS of: (i) bare Au, (ii) MBA/Au, (iii) $aAFB_1$-C-AuNP/MBA/Au and (iv) BSA/$aAFB_1$-C-AuNP/MBA/Au electrodes in PBS (50 mM, pH 7.4, 0.9% NaCl) solution containing 5 mM $[Fe(CN)_6]^{3-/4-}$.

3.4. Electrochemical characterization

Cyclic voltammetric studies (CV) have been conducted on (i) bare Au, (ii) MBA/Au, (iii) aAFB$_1$-C-AuNP/MBA/Au and (iv) BSA/aAFB$_1$-C-AuNP/MBA/Au electrodes in PBS containing 5 mM $[Fe(CN)_6]^{3-/4-}$, at a scan rate of 50 mV/s in the potential range of −0.75 to 0.75 V (Fig. 4(a)). The cyclic voltammogram of the bare gold shows oxidation and reduction peaks at 0.2 V and at 0.04 V, respectively (curve i). On treatment with MBA, the magnitude of peak current is found to decrease (curve ii) due to inhibition of the permeability of redox probe $[Fe(CN)_6]^{3-/4-}$ to the surface of electrode, indicating successful SAM formation of MBA onto gold electrode. The immobilization of aAFB$_1$-C-AuNP onto MBA/Au electrode results in decreased peak current (curve iii) with oxidation and reduction peaks at 0.53 V and −0.23 V respectively. This may be due to the hindrance caused by the aAFB$_1$-C-AuNP assembly to the flow of current. The magnitude of current further decreases after the immobilization of BSA (curve iv), owing to the blocking of non-specific sites present on the immunoelectrode that hinders the electron transfer between the medium and electrode. Similar results have been obtained in the DPV (Fig. 4(b)) and EIS (Fig. 4(c)) studies.

3.5. Electrochemical response studies

The results of response studies of BSA/aAFB$_1$-C-AuNP/MBA/Au immunoelectrode as a function of AFB$_1$ concentration investigated using CV and DPV techniques are shown in Fig. 5. The magnitude of current response is found to increase on addition of AFB$_1$ (Fig. 5(a) and (b)). This can be attributed to the formation of AFB$_1$–aAFB$_1$

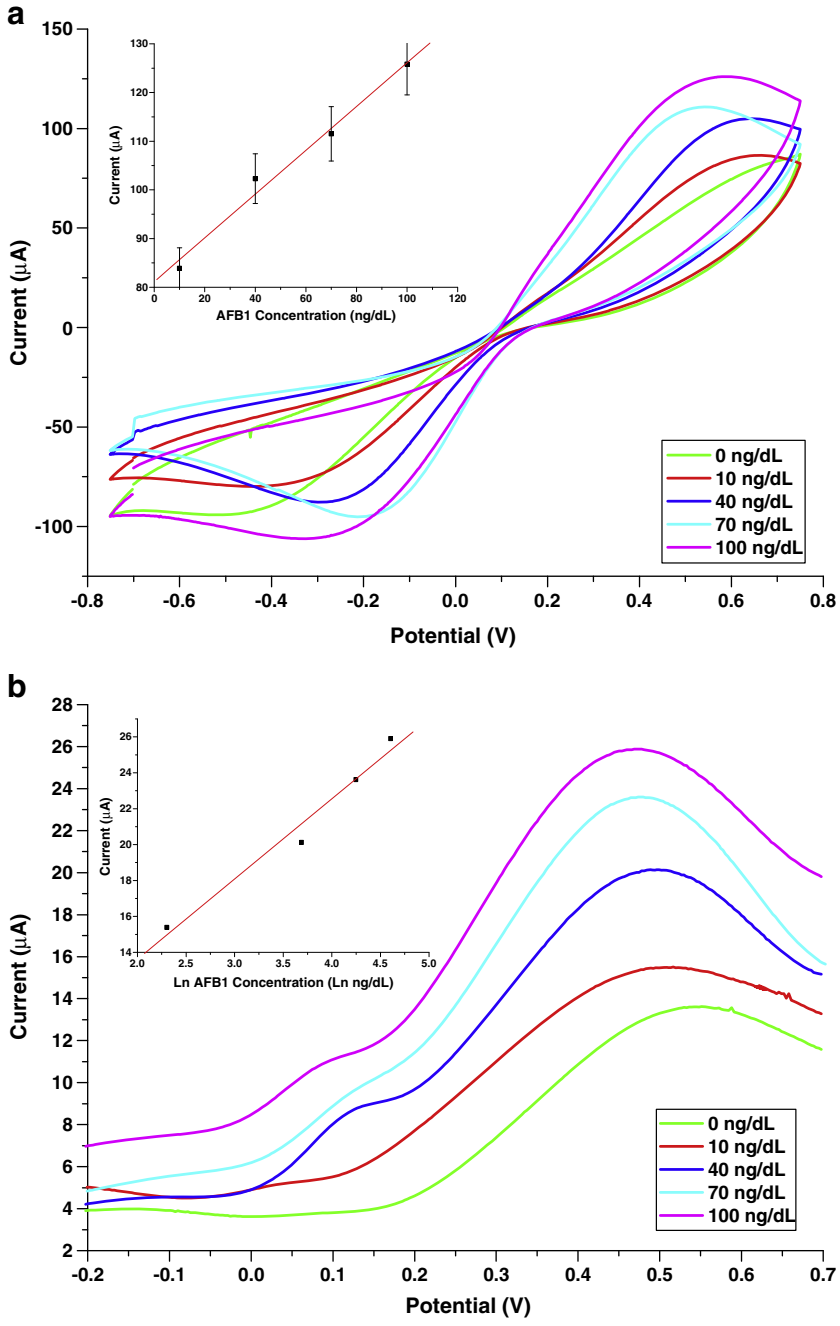

Fig. 5. (a) CV and (b) DPV recorded for BSA/aAFB$_1$-Cys-AuNP/CTP/Au immunoelectrode as a function of varying concentrations of AFB$_1$; 0 ng dL^{-1}, 10 ng dL^{-1}, 40 ng dL^{-1}, 70 ng dL^{-1}, and 100 ng dL^{-1}, in PBS (50 mM, pH 7.4, 0.9% NaCl) solution containing 5 mM $[Fe(CN)_6]^{3-/4-}$. [Inset shows calibration plots derived as a function of (a) AFB$_1$ and (b) ln (AFB$_1$) concentrations, from 0 to 100 ng dL^{-1}].

complex that might act as electron transfer-accelerating layer for the transfer of electrons [18,19]. The inset in Fig. 5(a) shows the calibration curve obtained as a function of AFB_1 concentration, using CV studies. It is observed that the peak current value is linearly proportional to AFB_1 concentration in the range between 10 and 100 ng dL^{-1} and follows Eq. (1).

$$I\,(\mu A) = 0.4498\left(\mu A ng^{-1} dL\right)\left[AFB_1\left(ngdL^{-1}\right)\right] + 81.1416(\mu A) \qquad (1)$$

with values of regression coefficient and standard deviation as 0.99217 and 2.68543 respectively. The value of sensitivity for this immunosensor using Eq. (1) is found to be 0.44983 μA ng^{-1} dL and the theoretical limit of detection (LOD) evaluated using equation $3s_{y/x}$/sensitivity (where $s_{y/x}$ is the standard deviation) [20] is 17.90 ng dL^{-1}. However, DPV studies indicate that the peak current increases exponentially as a function of AFB_1 concentration in the range of 10 ng dL^{-1} to 100 ng dL^{-1} (Fig. 5(b)) and follows the equation

$$I\,(\mu A) = 4.4665\left(\mu A ng^{-1} dL\right)\left[AFB_1\left(ngdL^{-1}\right)\right] + 4.6829(\mu A) \qquad (2)$$

with regression coefficient and standard deviation of 0.98649 and 0.91926 respectively.

4. Conclusions

An immunosensor based on antibody attached gold-nanoparticles has been fabricated for the detection of aflatoxin B_1. SEM studies show high surface coverage of the antibody onto the gold nanoparticles. Using cyclic voltammetric technique the prepared immunoelectrode is found to detect AFB_1 in the concentration range of 10 ng dL^{-1} to 100 ng dL^{-1}, with limit of detection as 17.90 ng dL^{-1}. The sensitivity of the immunoelectrode is found to be 0.45 μA ng^{-1} dL and 4.4 μA ng^{-1} dL by CV and DPV studies respectively, with a response time of 60 s.

Acknowledgements

We thank Prof. R. C. Budhani, Director, National Physical Laboratory, India, for providing the facilities. The authors thank Dr. K. N. Sood, NPL, for SEM measurements. Aditya Sharma is thankful to CSIR, India, for the award of a Junior Research Fellowship. The financial support received from Department of Biotechnology, India under the project GAP-080932, Department of Science and Technology, India (GAP-081132), in-House projects and the Ministry of Education, Science and Technology, Korea (R32-20026) are sincerely acknowledged.

References

[1] International Agency for Research on Cancer, IARC Monogr. Evaluations Carcinog. Risks Humans. IARC Lyon 56 (1993) 489.
[2] E. Anklam, J. Saroka, A. Boenke, Food Control 13 (2002) 173.
[3] D.M. Parkin, F. Bray, J. Ferlay, P. Pisani, Int. J. Cancer 94 (2001) 153.
[4] G.E. Wood, J. Assoc. Off. Anal. Chem. 72 (1989) 543.
[5] A. Fernandez, R. Belio, J.J. Ramos, M.C. Sanz, T. Saez, J. Sci. Food Agric. 74 (1997) 161.
[6] J. Jaimez, C.A. Fente, B.I. Vazquez, C.M. Franco, A. Cepeda, G. Mahuzier, P. Prognon, J. Chromatogr. A 882 (2000) 1.
[7] J. Stroka, E. Anklam, Trends Anal. Chem. 21 (2002) 90.
[8] J. Zhang, J. Wang, J. Zhu, J. Xu, H. Chen, D. Xu, Microchim. Acta 163 (2008) 63.
[9] Y. Bai, H. Yang, W. Yang, Y. Li, C. Sun, Sens. Actuators B 124 (2007) 179.
[10] P. Pandey, S.P. Singh, S.K. Arya, A. Sharma, M. Datta, B.D. Malhotra, J. Nanosci. Nanotechnol. 8 (2008) 3158.
[11] L. Tang, G.M. Zeng, G.L. Shen, Y.P. Li, Y. Zhang, D.L. Huang, Environ. Sci. Technol. 42 (2008) 1207.
[12] R.G. Discipio, Anal. Biochem. 236 (1996) 168.
[13] Y. Liu, Z. Qin, X. Wu, H. Jiang, Biochem. Eng. J. 32 (2006) 211.
[14] J.Y. Liao, Colloids Surf. B Biointerfaces 57 (1) (2007) 75.
[15] X. Jin, X. Jin, L. Chen, J. Jiang, G. Shen, R. Yu, Biosens. Bioelectron. 24 (8) (2009) 2580.
[16] R. Kojima, K. Mawatari, B. Renberg, T. Tsukahara, T. Kitamori, Microchim. Acta 164 (2009) 307.
[17] P. Pandey, S.P. Singh, S.K. Arya, V. Gupta, M. Datta, S. Singh, B.D. Malhotra, Langmuir 23 (2007) 3333.
[18] A. Kaushik, P.R. Solanki, A.A. Ansari, S. Ahmad, B.D. Malhotra, Electrochem. Commun. 10 (2008) 1364.
[19] A. Kaushik, P.R. Solanki, A.A. Ansari, S. Ahmad, B.D. Malhotra, Nanotechnology 20 (2009) 055105.
[20] J.C. Vidal, G.R. Espuelas, J.R. Castillo, Anal. Lett. 35 (5) (2002) 837.